

# Agent-Based Simulation of the Two-Dimensional Patlak-Keller-Segel Model

Gyu Ho Bae and Seung Ki Baek\*

*Department of Physics, Pukyong National University, Busan 48513, Korea*

The Patlak-Keller-Segel equation describes the chemotactic interactions of small organisms in the continuum limit, and a singular peak appears through spontaneous aggregation when the total mass of the organisms exceeds a critical value. To deal with this singular behavior numerically, we propose an agent-based simulation method in which both the organisms and the chemicals are represented as particles. Our numerical estimates for the threshold behavior are consistent with the analytic predictions.

PACS numbers: 02.60.Lj, 87.23.Cc

Keywords: Agent-based simulation, Patlak-Keller-Segel equation, Chemotaxis, Aggregation

## I. INTRODUCTION

Numerical approaches to a system of partial differential equations take up an important part of computational physics due to the wide range of applications from cosmology to quantitative finance. A variety of algorithms, such as those derived from the finite-difference and the finite-element methods [1–3], most of which are based on the differentiability of the solution, have been developed. However, as one sees from the inviscid Burger’s equation [4], some systems are known to develop singular behavior, which undermines the foundation of the existing numerical methods. Another example is the the Patlak-Keller-Segel (PKS) model that has been devised to describe chemotaxis, i.e., the movement of organisms in reaction to chemical stimulus [5–7]. As will be explained below, as the total mass of the organisms exceeds a certain threshold, the two-dimensional PKS model undergoes an aggregation transition by amplifying perturbations from a homogeneous solution, and all the mass eventually condenses into a single point. In other words, the mass density field develops a singularity at the transition, so the PKS model also poses a challenging problem in applying the existing numerical methods based on differentiability [8–10]. As an alternative, a proposal is to simulate organisms as particles whereas the chemical density is still represented by a continuous field [11], whose theoretical counterpart would be the many-body theory developed in Ref. 12.

The PKS model is worth investigating in its own right as a reaction-diffusion system for describing collective patterns [13]. Some examples include birds flying in a flock, a school of fish, swarms of insects, and ants forming a foraging path [14–16]. An interesting point about the previous examples is that those patterns are self-organized in the absence of a centralized leader in the community. Understanding the mechanism of such self-organization is both theoretically and practically important in biologically motivated fields of engineering, from biomechanics to swarm intelligence [17–20].

In this work, we propose analyzing the PKS model numerically in a fully agent-based fashion, i.e., treating both the organisms and the pheromones as particles. We will show that the numerical result is, indeed, consistent with the analytic prediction obtained in the continuum limit. The result will also be discussed in comparison with the semi-agent-based approach proposed in Ref. 11. This work is organized as follows: In the next section, we introduce some basic features of the PKS model. Section III explains our simulation method and presents the results. Discussing implications of the numerical results, we summarize this work in Section IV.

## II. MODEL

### 1. Patlak-Keller-Segel model

Here, we will explain the basic idea of the PKS model, following Refs. 21 and 22. Let  $\rho$  denote the number density of organisms confined in a  $d$ -dimensional domain called  $\Omega$ . The total number of organisms is a conserved quantity, so the variable  $\rho$  satisfies the continuity equation:

$$\frac{\partial \rho}{\partial t} + \nabla \cdot \mathbf{j} = 0. \quad (1)$$

The current  $\mathbf{j}$  has two contributions, one from the chemical gradient and the other from the random motions of the organisms. The former is proportional to  $\rho \nabla c$ , where  $c$  is the concentration of the chemical, and the latter is proportional to  $\nabla \rho$  as in the diffusion equation. Thus, we can write the total current as

$$\mathbf{j} = \chi_0 \rho \nabla c - \mu_0 \nabla \rho, \quad (2)$$

where  $\chi_0$  and  $\mu_0$  are positive constants denoting the organism’s chemotactic sensitivity and the diffusion coefficient, respectively. The density of the chemical changes through three processes: Namely, after having been deposited by the organisms, it diffuses to neighboring sites and decays stochastically with a certain rate by chemical degradation. Combining these three processes, we can

\* seungki@pknu.ac.kr; Fax: +82-51-629-5549

write the following equation:

$$\tau \frac{\partial c}{\partial t} = f_0 \rho + \nu_0 \nabla^2 c - g_0 c, \quad (3)$$

where  $\tau$  is a dimensionless parameter to set the relative time scale of the chemical dynamics with respect to that of the organism's dynamics, and  $f_0$ ,  $g_0$ , and  $\nu_0$  are positive constants to denote the specific rates of pheromone deposition, diffusion, and degradation, respectively. To sum up, the PKS model can be described as follows:

$$\frac{\partial \rho}{\partial t} = -\chi_0 \nabla \cdot (\rho \nabla c) + \mu_0 \nabla^2 \rho, \quad (4a)$$

$$\tau \frac{\partial c}{\partial t} = f_0 \rho + \nu_0 \nabla^2 c - g_0 c. \quad (4b)$$

We impose the Neumann boundary conditions  $\nabla \rho \cdot \hat{n} = \nabla c \cdot \hat{n} = 0$  at the boundary  $\partial\Omega$ , where  $\hat{n}$  denotes the normal vector to  $\partial\Omega$ . This means that the normal component of the density gradient vanishes everywhere at the boundary, so that the flux across the boundary is zero. Due to the boundary conditions, the total mass  $M \equiv \int_{\Omega} \rho \, d\mathbf{r}$  is conserved, where  $\mathbf{r}$  denotes the  $d$ -dimensional position vector.

## 2. Power counting

By using a power counting argument, one can argue that the aggregation phenomenon described by Eq. (4) has a critical dimension  $d_c = 2$ , below which the population cannot spontaneously collapse into a single point [22]. Suppose that a  $d$ -dimensional aggregate has a linear size denoted by  $\xi$ . The number density is then  $\rho \sim \xi^{-d}$ , and the differential operator has  $\nabla \sim \xi^{-1}$ . The deposition of the chemical is proportional to  $\rho$ ; hence,  $\partial c / \partial t \sim \xi^{-d}$ . If  $c$  is on the order of  $\xi^{-\alpha}$  and the dynamics has a time scale of  $t \sim \xi^\beta$ , then

$$\alpha + \beta = d. \quad (5)$$

The left-hand side of Eq. (4a) is, thus, on the order of  $\xi^{-(d+\beta)}$  whereas the two terms on the right-hand side (RHS) scale as  $\xi^{-(2+d+\alpha)}$  and  $\xi^{-(2+d)}$ , respectively. Note that the former one is responsible for aggregation while the latter describes diffusion. We assume that the dominant process is aggregation so that

$$d + \beta = 2 + d + \alpha. \quad (6)$$

By solving Eqs. (5) and (6) together, we obtain

$$\begin{cases} \alpha = \frac{d}{2} - 1, \\ \beta = \frac{d}{2} + 1. \end{cases} \quad (7)$$

As a consequence, the two terms on the RHS of Eq. (4a) scale as  $\xi^{-(1+3d/2)}$  and  $\xi^{-(2+d)}$ , respectively. If we consider the limit of  $\xi \rightarrow 0$ , the description of aggregation remains self-consistent when  $d > 2$ , for which  $1 + 3d/2 >$

$2 + d$ . At the critical dimension  $d = 2$ , the competition between aggregation and diffusion should be determined by using higher-order terms, and a threshold of the total mass of organisms for aggregation to take place, as explained below, turns out to exist.

## 3. Linear stability analysis in two dimensions

Let us consider a homogeneous solution  $\rho = \frac{g_0}{f_0} c = \rho_{\text{const}}$  on a square plane  $\Omega = [0, L] \times [0, L]$ . We examine the linear stability of the solution when small perturbations are added, i.e.,  $\rho(x, y, t) = \rho_{\text{const}} + \epsilon_\rho(x, y, t)$  and  $c(x, y, t) = \frac{f_0}{g_0} \rho_{\text{const}} + \epsilon_c(x, y, t)$ . Due to the boundary conditions, the perturbations can be written as

$$\epsilon_\rho(x, y, t) = C_1 \cos \frac{m\pi x}{L} \cos \frac{n\pi y}{L} e^{\eta t}, \quad (8a)$$

$$\epsilon_c(x, y, t) = C_2 \cos \frac{m\pi x}{L} \cos \frac{n\pi y}{L} e^{\eta t}, \quad (8b)$$

with integers  $m$  and  $n$ , from which we obtain

$$\eta \begin{pmatrix} C_1 \\ C_2 \end{pmatrix} = \begin{pmatrix} -k^2 \mu_0 & k^2 \chi_0 \rho_{\text{const}} \\ f_0 & -g_0 - k^2 \nu_0 \end{pmatrix} \begin{pmatrix} C_1 \\ C_2 \end{pmatrix}, \quad (9)$$

with  $k \equiv (\pi/L)\sqrt{m^2 + n^2}$ . For such perturbations to grow in time with  $\eta > 0$ , one needs the following inequality:

$$\mu_0 [g_0 + \pi^2 (m^2 + n^2) \nu_0 / L^2] - f_0 \chi_0 \rho_{\text{const}} < 0. \quad (10)$$

The resulting mass of the organisms is

$$M = \rho_{\text{const}} L^2 \quad (11)$$

$$> \frac{\mu_0 g_0}{f_0 \chi_0} L^2 + \pi^2 (m^2 + n^2) \frac{\mu_0 \nu_0}{f_0 \chi_0} \quad (12)$$

$$\approx \pi^2 (m^2 + n^2) \lambda, \quad (13)$$

where  $g_0$  is assumed to be negligibly small, and we have defined

$$\lambda \equiv \mu_0 \nu_0 / (f_0 \chi_0). \quad (14)$$

The mass for the lowest order perturbation to make a homogeneous solution become unstable is, therefore,

$$M_c = \pi^2 \lambda. \quad (15)$$

## 4. Bistability

Let us now consider an inhomogeneous stationary solution of Eqs. (4a) and (4b) for  $d = 2$  [22]. For the sake of analytic tractability, we assume that the aggregate is formed in the middle of a large two-dimensional plane. The system may, thus, be approximated as having radial symmetry so that the solution has only an  $r$ -dependence in polar coordinates. In a stationary state, the boundary conditions imply that  $\mathbf{j} = 0$  everywhere. Then, we have

$$\chi_0 \rho \nabla c - \mu_0 \nabla \rho = 0, \quad (16)$$

for which the solution is

$$\rho = R \exp(\tilde{c}), \quad (17)$$

where  $R$  is a positive constant and  $\tilde{c} \equiv (\chi_0/\mu_0)c$ . Substituting Eq. (17) into Eq. (4b), we obtain

$$0 = \lambda^{-1} R \exp(\tilde{c}) + \nabla^2 \tilde{c}, \quad (18)$$

where we have discarded the decay term by taking the small- $g_0$  limit. This is Liouville's equation, and it has a solution of the following form [23]:

$$\lambda^{-1} R \exp(\tilde{c})(u^2 + v^2 + 1)^2 = 2 \left[ \left( \frac{\partial u}{\partial x} \right)^2 + \left( \frac{\partial u}{\partial y} \right)^2 \right], \quad (19)$$

where  $F(z) = u(x, y) + iv(x, y)$  is an arbitrary analytic function with  $z = x + iy$ . If  $u/x = v/y = \text{const.}$ , we have a radially symmetric aggregate:

$$\rho(r) = \rho_0 \left( 1 + \frac{\rho_0}{8\lambda} r^2 \right)^{-2}, \quad (20)$$

with  $r \equiv \sqrt{x^2 + y^2}$  and  $\rho_0 \equiv \rho(r=0)$ . Even if we impose radial symmetry, the equation admits an infinite number of different solutions, including annular shapes [23]. Among them, Eq. (20) has a characteristic length scale  $\xi \sim \int_0^\infty \rho(r)r^2 dr / \int_0^\infty \rho(r)r dr = \pi\sqrt{2\lambda/\rho_0}$  so that  $\rho_0 \propto \xi^{-2}$ , in agreement with the above power counting argument. The total mass of the organisms in this stationary state is

$$M_0 = 2\pi \int_0^\infty \rho(r)r dr = 8\pi\lambda. \quad (21)$$

If an aggregate is allowed to form at one of the corners of  $\Omega$ , as is often the case in numerical simulations, considering the four-fold symmetry, the mass for a stationary aggregate should be counted as a fourth of Eq. (21) [11]. We note that the solution becomes exceedingly complicated on a bounded domain with other boundary conditions (see, e.g., Ref. 24). However, if we have a sufficiently large  $L$  compared to the width of the aggregate, we may expect this kind of calculation still to give a reasonable estimate. On the other hand, we have seen that the homogeneous solution is linearly stable up to  $M = \pi^2\lambda$  [Eq. (15)]. This suggests that the system will be bistable when

$$2\pi\lambda \lesssim M \lesssim \pi^2\lambda. \quad (22)$$

## 5. Coarsening of aggregates

Depending on the initial condition, the system may develop multiple aggregates, and the question is then how these aggregates interact with one another [25, 26]. An instructive assumption would be for the chemical dynamics to be fast enough to set  $\tau = 0$  in Eq. (4b) [11]. We

then obtain an inhomogeneous modified Helmholtz equation,

$$(\nabla^2 - \kappa^2) c = -\frac{f_0}{\nu_0} \rho. \quad (23)$$

where  $\kappa^{-1} \equiv \sqrt{\nu_0/g_0}$  defines a length scale, meaning how far the chemical travels before decaying at time  $\sim g_0^{-1}$ . The formal solution is given by a convolution formula,

$$c(\mathbf{x}, t) = -\frac{f_0}{\nu_0} (\mathcal{G} * \rho)(\mathbf{x}, t) = -\frac{f_0}{\nu_0} \int d\mathbf{y} \mathcal{G}(\mathbf{x} - \mathbf{y}) \rho(\mathbf{y}, t), \quad (24)$$

with a Green's function  $\mathcal{G}$ . In two dimensions, it takes the following form:

$$\mathcal{G}(\mathbf{x}) = -\frac{K_0(\kappa x)}{2\pi}, \quad (25)$$

where  $K_0$  is the modified Bessel function of the second kind. For a small argument  $z \ll 1$ , it can be approximated as

$$K_0(z) \approx -\gamma - \ln\left(\frac{z}{2}\right), \quad (26)$$

where  $\gamma \approx 0.5772$  is the Euler-Mascheroni constant. Such logarithmic behavior at a short distance is a signature of two-dimensional gravity, and this behavior crosses over to an exponential decay as the distance exceeds  $\kappa^{-1}$ . Substituting Eq. (24) into Eq. (4a), we get a closed equation for  $\rho$ ,

$$\frac{\partial \rho}{\partial t} = \nabla \cdot \left[ \frac{f_0 \chi_0}{\nu_0} \rho \nabla (\mathcal{G} * \rho) + \mu_0 \nabla \rho \right] = \nabla \cdot \left[ \rho \nabla \frac{\delta \mathcal{E}}{\delta \rho} \right], \quad (27)$$

with

$$\mathcal{E}[\rho(\mathbf{x})] \equiv \mu_0 \int \rho(\mathbf{x}) \ln \frac{\rho(\mathbf{x})}{\rho_{\text{ref}}} d\mathbf{x} + \frac{f_0 \chi_0}{2\nu_0} \iint \rho(\mathbf{x}) \mathcal{G}(\mathbf{x} - \mathbf{y}) \rho(\mathbf{y}) d\mathbf{x} d\mathbf{y}, \quad (28)$$

where  $\rho_{\text{ref}}$  is a constant to make the argument of the logarithm dimensionless.

Equation (27) describes relaxational dynamics, in which the functional  $\mathcal{E}$  is non-increasing:

$$\frac{d\mathcal{E}}{dt} = \int \frac{\partial \rho(\mathbf{x})}{\partial t} \frac{\delta \mathcal{E}}{\delta \rho} d\mathbf{x} \quad (29)$$

$$= \int \nabla \cdot \left( \rho \nabla \frac{\delta \mathcal{E}}{\delta \rho} \right) \frac{\delta \mathcal{E}}{\delta \rho} d\mathbf{x} \quad (30)$$

$$= - \int \left| \nabla \frac{\delta \mathcal{E}}{\delta \rho} \right|^2 \rho(\mathbf{x}) d\mathbf{x} \leq 0, \quad (31)$$

where we have used integration by parts in deriving the last line. This inequality shows that  $\mathcal{E}$  is a Lyapunov functional (see also Refs. 27–29). If we interpret Eq. (28) as the free energy in the limit of fast pheromone dynamics, the first and the second terms will correspond to its entropic and energetic contributions, respectively. The latter part suggests that the interaction potential between positions  $\mathbf{x}$  and  $\mathbf{y}$  is given by the Green's function  $\mathcal{G}(\mathbf{x} - \mathbf{y})$ , which essentially describes two-dimensional gravity with a finite range of interaction,  $\kappa^{-1}$ .

### III. METHOD AND RESULT

Let us begin this section by reviewing the numerical approach of Ref. 11 in which organisms are represented as particles whereas the chemical density  $c$  is represented as a field variable defined at each lattice point. This choice may be justified by the fact that  $c$  exhibits a weaker divergence than  $\rho$  [see Eq. (17)]. The number of particles is  $N$ , so each particle carries mass  $m \equiv M/N$ . The position of the  $n$ th particle is denoted by  $X^{(n)}$ , and it is updated by chemotaxis and diffusion by using the explicit Euler scheme

$$X^{(n)}(t+\Delta t) = X^{(n)}(t) + \chi_0 \nabla c \Delta t + \sqrt{2\mu_0 \Delta t} \mathcal{N}(0, 1), \quad (32)$$

where  $\mathcal{N}(0, 1)$  means a random number drawn from the Gaussian distribution with zero mean and unit variance. The author of Ref. 11 argued that the empirical probability density for  $X^{(n)}$  converges to  $\rho$ , satisfying Eq. (4a), as  $N \rightarrow \infty$ . Numerically, the mass density field  $\rho$  is reconstructed from the set of  $X^{(n)}$ 's through bilinear interpolation. It is then used as an input to solve a system of coupled linear equations, a lattice-discretized version of Eq. (4b), by using an implicit method. As in Section II 3, we consider  $\Omega = [0, L] \times [0, L]$  throughout this section, and the reflecting boundary condition is imposed to simulate the Neumann boundaries at the particle level.

The difference of our method lies in the way we deal with the chemical density field  $c$ . Here, the chemicals are also represented as particles, and their dynamics consists of three parts: deposition, diffusion, and degradation [Eq. (4b)]. First, an organism particle (OP) deposits a pheromone particle (PP) with probability  $f_0 \Delta t / \tau$  at each time step. Observing that the deposition rate is proportional to the mass density of the organisms, not to the number density of OP's, is important. This implies that we need to consider the dynamics in terms of *mass* so that each PP should also carry the weight of  $m$  just as an OP does. The number of PP's is not conserved during the simulation. Let  $Y^{(n)}$  denote the position of the  $n$ th PP. This variable is updated by diffusion, again by using the explicit Euler scheme

$$Y^{(n)}(t + \Delta t) = Y^{(n)}(t) + \sqrt{2\nu_0 \Delta t / \tau} \mathcal{N}(0, 1). \quad (33)$$

Finally, the pheromone particle is eliminated with probability  $g_0 \Delta t / \tau$ .

In simulations, we take different numbers of OP's:  $N = 100, 400, \text{ and } 1000$ . We also need to set the number of grid cells along each direction,  $B$ , to reconstruct the density fields  $\rho$  and  $c$ . Our criterion is that the number of grid cells in  $\Omega$  should be smaller than or comparable to that of the OP's, i.e.,  $B^2 \lesssim N$ . We check different values of  $m$ , the mass of each OP, to see how the system's behavior changes as the total mass  $M$  varies while keeping  $N$  constant. For each  $M$ , we generate six independent samples and run the simulations up to  $t = O(10^4)$ . The initial condition is based on a uniformly random distribution of OP's with no PP's, and a bias toward the origin has been added as a perturbation, following Ref. 11.

For the modeling parameters, we choose  $\mu_0 = 5 \times 10^{-3}$ ,  $\nu_0 = 1$ ,  $\chi_0 = 10^{-1}$ ,  $g_0 = 10^{-2}$ ,  $f_0 = 1$ , and  $\tau = 10^{-1}$ . This gives us  $\lambda \equiv \mu_0 \nu_0 / (f_0 \chi_0) = 5 \times 10^{-2}$  [Eq. (14)]. The size of  $\Omega$  is given by  $L = 3.2$ , and the time step is  $\Delta t = 10^{-3}$ . We use this  $\Delta t$  so that the displacement of each PP in Eq. (33) does not exceed the lattice constant  $a \equiv L/B$ . A chemotactic interaction can, nevertheless, cause an OP's displacement to be greater than  $a$  with this  $\Delta t$ . Therefore, we have additionally implemented the adaptive time-stepping method as proposed in Ref. 11: If the displacement of the  $n$ th OP becomes greater than  $a$ , we subdivide  $\Delta t$  into smaller pieces, e.g., 10 pieces of  $\Delta t/10$ , and find  $X^{(n)}(t + \Delta t)$  by updating  $X^{(n)}(t)$  ten times with this smaller time interval,  $\Delta t/10$ . Just as we do for  $\rho$ , we reconstruct the chemical density field  $c$  through bilinear interpolation of the positions of the PP's, which is then used as an input to calculate the RHS of Eq. (32).

Our main observable is defined as follows:

$$\Sigma_M \equiv \frac{1}{M^2} \int_{\Omega} \rho^2(\mathbf{r}) \, d\mathbf{r}, \quad (34)$$

where the prefactor is necessary for adjusting the trivial dependence on  $M$  even when the distribution keeps the same shape. The more evenly the distribution  $\rho$  spreads, the smaller the value of  $\Sigma_M$  takes. This observable is related to the participation ratio in the localization problem [30] and is commonly used to measure inhomogeneity [31]. Numerically, the integral is calculated with the Riemann sum over the lattice points.

To check our approach, we have reproduced the method of Ref. 11, in which only the organisms are represented as particles. The result is shown in Fig. 1(a), and it is qualitatively consistent with the analytically predicted bistable behavior in Eq. (22). Based on this existing method, we have implemented our own, as explained above. The result is depicted in Fig. 1(b), which is also in good agreement with the analytic prediction. The thresholds can readily be estimated from these numerical results, and the estimates for the upper threshold,  $M_c = \pi^2 \lambda \approx 0.493$ , are shown in Fig. 2. The size dependence is small, and no big difference is observed between  $N = 400$  and 1000. Compared to the pheromone-field method in Ref. 11, we see that our pheromone-particle method gives a better estimate for the upper threshold.

### IV. DISCUSSION AND SUMMARY

In this work, we have proposed solving the PKS model numerically in a fully agent-based fashion to simulate its singular behavior of aggregation. We have found that our simulation method successfully reproduces the analytic predictions. In Eq. (22), we have estimated the bistable region. With our parameter values, the upper threshold is given as  $M_c = \pi^2 / \lambda \approx 0.493$ . We have estimated the upper threshold as being as somewhere between 0.47 and 0.50 (Fig. 2). We also observe a qualitatively consistent

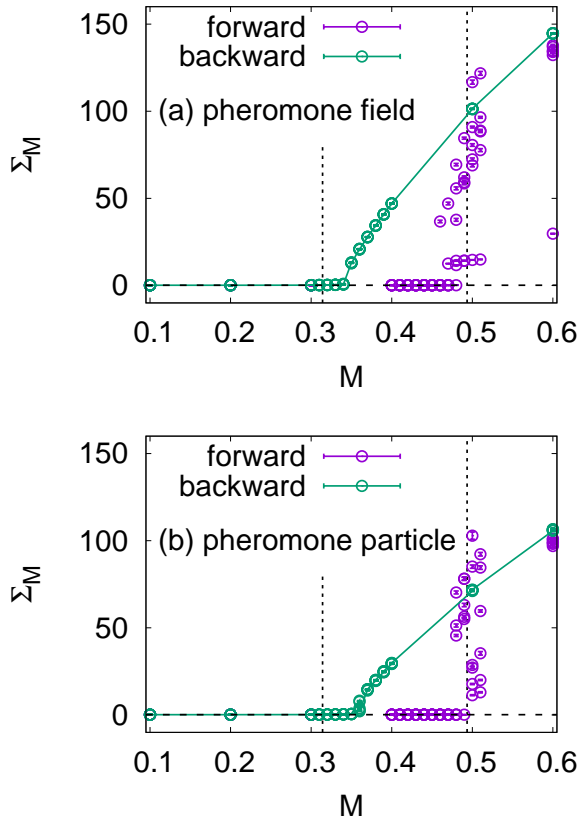


Fig. 1.  $\Sigma_M$  versus  $M$  at  $t = 3 \times 10^4$  when  $N = 10^3$  and  $B = 32$ . For the modeling parameters, we choose  $\mu_0 = 5 \times 10^{-3}$ ,  $\nu_0 = 1$ ,  $\chi_0 = 10^{-1}$ ,  $g_0 = 10^{-2}$ ,  $f_0 = 1$ , and  $\tau = 10^{-1}$ . This gives us  $\lambda \equiv \mu_0 \nu_0 / (f_0 \chi_0) = 5 \times 10^{-2}$  [Eq. (14)]. The size of  $\Omega$  is given by  $L = 3.2$ , and the time step is  $\Delta t = 10^{-3}$ . We take six independent samples for each  $M$ . By ‘forward’ and ‘backward’, we mean that  $M$  is increased and decreased, respectively, after reaching a steady state for given  $M$ . (a) Results from the method in Ref. 11 where pheromones are represented as a field variable  $c$  defined at each lattice point, and (b) those from our method, where pheromones are represented as particles. The horizontal dashed lines mean  $\Sigma_M$  for  $N$  randomly distributed points, and the vertical dotted lines mean the analytic thresholds in Eq. (22), i.e.,  $2\pi\lambda \approx 0.314$  and  $\pi^2/\lambda \approx 0.493$ .

result by using the pheromone-field method in Ref. 11. However, if we look more closely, this latter method tends to underestimate the threshold as one sees in Fig. 2. A possible explanation for this deviation could be that the diffusion coefficient  $\mu_0$  is renormalized when the continuum limit is taken for  $c$  first [12]: The perturbative calculation is based on an assumption that  $\nu_0 \gg \mu_0$ , which is valid in our case where  $\nu_0/\mu_0 = 2 \times 10^2$ . The correction terms involve a cutoff length called  $\Lambda$ . If we take it as being identical to the lattice constant  $a = 10^{-1}$  for  $N = 10^3$  and calculate the correction to the second order as given in Ref. 12, the corresponding threshold value is lowered to 0.454. On the other hand, the bare parameter values are preserved if one takes the limiting process

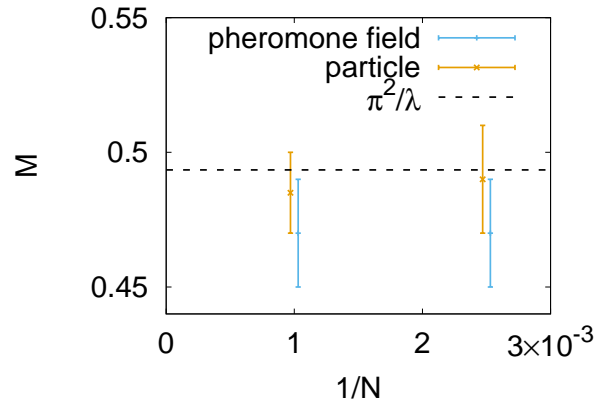


Fig. 2. Threshold estimates from the two numerical methods: One is proposed in Ref. 11 where pheromones are represented as field variables, and the other is ours, where pheromones are represented as particles. The horizontal dashed line is the predicted upper threshold from the linear stability analysis,  $M_c = \pi^2\lambda \approx 0.493$  [Eq. (15)]. We are not showing the results for  $N = 100$ , where both the methods yield equally imprecise estimates because of large statistical fluctuations in particle dynamics.

simultaneously for  $\rho$  and  $c$  [32].

The lower threshold in Eq. (22) is more difficult to check. It has been estimated to be  $M_0 = 2\pi\lambda \approx 0.314$  from the stationarity of an aggregate. Our numerical approach shows that the aggregation persists until the mass decreases to  $M = 0.36$ , but this is still greater than the analytic prediction. This is presumably because the calculation in Section II 4 is based on an assumption that  $\Omega$  is an unbounded plane  $\mathbb{R}^2$ . We are working with a finite square domain throughout this work, so the threshold can plausibly become greater than in  $\mathbb{R}^2$ . The reason is as follows: As discussed in Section II 5, our system can be regarded as a gravitational model, and the method of images under the Neumann boundary condition suggests that an organism and its image will also interact each other. In effect, therefore, an organism will experience an attractive interaction toward the boundary, which is expected to disperse an aggregate. This implies that the mass required for a stationary aggregate in  $\mathbb{R}^2$  may not be enough when it comes to a finite domain. If we alternatively look for the minimum mass required for an organism not to escape from the neighborhood of  $\rho(r) = M\delta(r)$ , where  $\delta$  is the Dirac delta distribution, the lower threshold decreases further down to  $\pi\lambda \approx 0.157$  (see Ref. 11 for calculating this threshold through a mapping to the Bessel process). Again, this value has been derived for  $\mathbb{R}^2$ , and our simulation was unable to detect this threshold within the bounded region.

In the context of chemotaxis, the fully agent-based method is intuitively plausible because, in a sense, it brings us back to the starting point of the PKS model before taking the continuum limit (see, e.g., Ref. 32 for the derivation of the PKS model as a limit of a stochastic

particle system), but the point is that it tells us how to analyze a given PDE system while keeping its numerical instability suppressed in a more general context. As one can anticipate, this agent-based method is usually less efficient than the existing method in Ref. 11, especially when the specific pheromone deposition rate is high. Developing a hybrid method to combine the advantages of the two methods would be desirable.

## ACKNOWLEDGMENTS

This work was supported by a research grant from Pukyong National University (2017).

## REFERENCES

- [1] M. E. J. Newman, *Computational Physics* (CreateSpace Independent, San Bernardino, CA, 2013).
- [2] D. L. Logan, *A first course in the finite element method* (Thomson, Australia, 2007).
- [3] S. K. Baek and M. Kim, *J. Korean Phys. Soc.* **71**, 1 (2017).
- [4] G. B. Whitham, *Linear and nonlinear waves*, Vol. 42 (John Wiley & Sons, New York, 2011).
- [5] C. S. Patlak, *Bull. Math. Biophys.* **15**, 311 (1953).
- [6] E. F. Keller and L. A. Segel, *J. Theor. Biol.* **26**, 399 (1970).
- [7] D. Horstmann, *Jahresber. Dtsch. Math. Ver.* **105**, 103 (2003); **106**, 51 (2004).
- [8] Y. Epshteyn, *J. Comput. Appl. Math.* **224**, 168 (2009); Y. Epshteyn and A. Izmirliglu, *J. Sci. Comput.* **40**, 211 (2009); Y. Epshteyn and A. Kurganov, *SIAM J. Numer. Anal.* **47**, 386 (2008).
- [9] N. Saito, *IMA J. Numer. Anal.* **27**, 332 (2007).
- [10] R. Strehl, A. Sokolov, D. Kuzmin, and S. Turek, *Comput. Meth. Appl. Math.* **10**, 219 (2010).
- [11] I. Fatkullin, *Nonlinearity* **26**, 81 (2012).
- [12] T. Newman and R. Grima, *Phys. Rev. E* **70**, 051916 (2004).
- [13] T. Vicsek, *Phys. Rev. Lett.* **75**, 1226 (1995); A. Czirók, E. Ben-Jacob, I. Cohen, and T. Vicsek, *Phys. Rev. E* **54**, 1791 (1996); T. Vicsek and A. Zafeiris, *Phys. Rep.* **517**, 71 (2012).
- [14] B. Hölldobler and E. O. Wilson, *The Ants* (The Belknap Press, Cambridge, 1990).
- [15] G. Sempo, S. Depickère, and C. Detrain, *Behav. Ecol.* **17**, 642 (2006).
- [16] J. Oettler, V. S. Schmid, N. Zankl, O. Rey, A. Dress, and J. Heinze, *PLoS ONE* **8**, 1 (2013).
- [17] J. Deneubourg, S. Goss, N. Franks, A. Sendova-Franks, C. Detrain, and L. Chrétien, in *From animals to animats: Proceedings of the first international conference on simulation of adaptive behavior*, edited by J.-A. Meyer and S. W. Wilson (MIT Press, Cambridge, MA, 1991) pp. 356–363.
- [18] M. Dorigo and T. Stützle, *Ant Colony Optimization* (A Bradford Book, London, 2004).
- [19] O. A. Mohamed Jafar and R. Sivakumar, *Int. J. Comput. Theor. Eng.* **2**, 1793 (2010).
- [20] M. Tenenbaum, Z. Liu, D. Hu, and A. Fernandez-Nieves, *Nat. Mater.* **15**, 54 (2015).
- [21] V. Nanjundiah, *J. Theor. Biol.* **42**, 63 (1973).
- [22] S. Childress and J. K. Percus, *Math. Biosci.* **56**, 217 (1981).
- [23] G. Walker, *Proc. R. Soc. Lond. A* **91**, 410 (1915).
- [24] E. Tracy, C. Chin, and H. Chen, *Physica D* **23**, 91 (1986).
- [25] J. J. L. Velázquez, *SIAM J. Appl. Math.* **64**, 1198 (2004); **64**, 1224 (2004).
- [26] J. Dolbeault and C. Schmeiser, *Discrete Contin. Dyn. Syst. B* **25**, 109 (2009).
- [27] P. Biler, *Adv. Math. Sci. Appl.* **8**, 715 (1998).
- [28] V. Calvez and L. Corrias, *Commun. Math. Sci.* **6**, 417 (2008).
- [29] S. K. Baek and B. J. Kim, *Sci. Rep.* **7**, 8909 (2017); G. H. Bae and S. K. Baek, *Phys. Rev. E* **100**, 022605 (2019).
- [30] J. T. Edwards and D. J. Thouless, *J. Phys. C* **5**, 807 (1972).
- [31] M. J. Lee, W. S. Jo, I. G. Yi, S. K. Baek, and B. J. Kim, *Physica A* **443**, 415 (2016).
- [32] A. Stevens, *SIAM J. Appl. Math.* **61**, 183 (2000).